Article

Corrosion Behaviors of Tetrasodium Iminodisuccinate (IDS) as an Environmentally Friendly Inhibitor: Experimental and Theoretical Studies

Shaopeng Fu [1], Xingyao Yang [1], Yichun Peng [2,*], Qi Wang [1], Qinghao Sun [1], Junwei Zhang [2], Xinping Wang [2], Zezhou Liang [3] and Jianfeng Li [1,*]

[1] School of Materials Science and Engineering, Lanzhou Jiaotong University, Lanzhou 730070, China
[2] School of Civil Engineering, Lanzhou Institute of Technology, Lanzhou 730050, China
[3] School of Electronics Science & Engineering, Faculty of Electronic and Information Engineering, Xi'an Jiaotong University, Xi'an 710049, China
* Correspondence: pengyc@lzit.edu.cn (Y.P.); ljfpyc@163.com (J.L.)

Abstract: An environmentally friendly chelating agent, tetrasodium iminodisuccinate (IDS), was investigated as an inhibitor in the simulated concrete pore solution on Q235 carbon steel by using Tafel polarization (TF), electrochemical impedance spectroscopy (EIS) and surface morphology tests. The EIS and TF results indicate that the IDS is a mixed type of inhibitor and exhibits excellent protection efficiency (97.54%) at 200 mg/L. Furthermore, based on the Langmuir adsorption isotherm, IDS protects carbon steel through physical and chemical adsorption. Besides, density functional theory (DFT) and molecular dynamics (MD) simulations are applied to explore the inhibition mechanism to support the experimental data, indicating that IDS can be used as a new green corrosion inhibitor.

Keywords: tetrasodium iminodisuccinate (IDS); corrosion inhibitor; electrochemical measurements; Q235 carbon steel

1. Introduction

The durability of reinforced concrete structures mainly depends on the corrosion resistance of the reinforcement, which is related to the passivation film on the surface [1,2]. When aggressive ions (Cl^-) enter the reinforced concrete structure, the passivation film will be damaged, and the concrete reinforcement will be eroded by chloride ions and then gradually corrode. Adding inhibitors is an important way to inhibit corrosion [3–5]. The research of inhibitors exhibited significant theoretical and practical implications for corrosion and protection of steel reinforcement.

It is reported that many traditional inorganic corrosion inhibitors have been banned because of their toxic and hazardous nature [6,7]. Organic compounds containing N, O, S, and P commonly all exhibit good corrosion inhibition properties [8–10]. However, many organic inhibitors are expensive and harmful to the environment. Therefore, many researchers have extracted effective substances from natural plants as green corrosion inhibitors. Still, there are limitations, including the complexity of the extraction process, low inhibition efficiency and few active ingredients found to contribute to corrosion inhibition [11]. Therefore, the search for environmentally friendly, safe, non-toxic, easily degradable, and efficient corrosion inhibitors has recently become a major research direction [12].

Tetrasodium iminodisuccinate (IDS) is a new type of amino acid chelating agent that is completely biodegradable, non-toxic, water-soluble and has a strong chelating ability, especially for iron and copper metal ions. Tetrasodium iminodisuccinate (IDS) is derived from succinic acid, a water-soluble compound. There have been many studies on structural design based on succinic acid (SA). For example, polyepoxy succinic acid (PESA) has good chelating properties, which exhibited excellent inhibition in alkaline

solutions as a green inhibitor [13]. And the mechanism of ethylenediamine-tetraacetic acid was investigated. Both the EIS results (83%) and the potentiodynamic test (85%) results indicated that ethylenediamine-tetraacetic acid exhibited the best corrosion protection at 0.05 M [14]. Furthermore, Teymouri et al. analyzed four carboxylate derivatives in simulated concrete pore solutions with 0.5 M NaCl for comparative purposes, and the test results showed that Trisodium Citrate (Cit) performed the highest corrosion inhibition at 0.1 M (91%) [15].
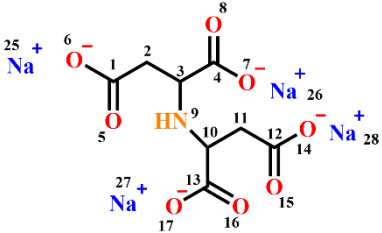
This work investigated the effect of tetrasodium iminodisuccinate (IDS) as a green inhibitor. Different concentrations of IDS were used, and different ambient temperatures were simulated. The inhibition efficiency and mechanism of IDS were studied by combining electrochemical tests, surface morphology tests, DFT calculations and MD simulations.

2. Materials and Methods

2.1. Experimental Materials and Test Solutions

In this work, we used tetrasodium iminodisuccinate (AR), as detailed in Table 1, and the simulated concrete pore solution with the following composition: 3.5% NaCl, 0.65 mol/L KOH, 0.15 mol/L NaOH and saturated $Ca(OH)_2$ solution (All chemicals in this work are analytically pure). The working electrode (Q235 carbon steel) is prepared as follows. Firstly, weld the carbon steel to the copper wire. The length of the wire exposed at the welded end should not be too long. Then, place it in a PVC pipe of appropriate length and diameter. The exposed surface as the working surface, and the working area is 1 cm^2. The carbon steel and PVC pipe were sealed with epoxy resin filling and placed in a dry and ventilated place. After fixing the shape, use 80#–2000# type sandpaper to sand the test surface, then polish it until it is smooth and flat. Then rinsed with deionized water and wiped using anhydrous ethanol.

Table 1. Chemical characterizations of IDS.

Parameter	Description
Molecular Structure	
Appearance	White powder
pH (1% water solution)	11
Molecular formula	$C_8H_7NNa_4O_8$
Molecular weight	337.10200

2.2. Electrochemical Testing

The instrument used for the tests is an electrochemical workstation (ChenHua CHI660E, Shanghai, China), as shown in Figure 1. The materials of the three electrodes were platinum sheet (auxiliary electrode), saturated glycerol (reference electrode) and Q235 carbon steel (working electrode) [16,17]. The open circuit potential (E_{OCP}) was first measured for 1 h. Secondly, the impedance spectra were tested in the frequency range from 100 kHz to 10 mHz and at an AC amplitude of 10 mV. Resolving with Zview software (2.70). Finally, Tafel curves were tested on Q235 carbon steel with polarization potentials ranging from −250 to +250 mV relative to the open circuit potential at a scan rate of 1 mV/s.
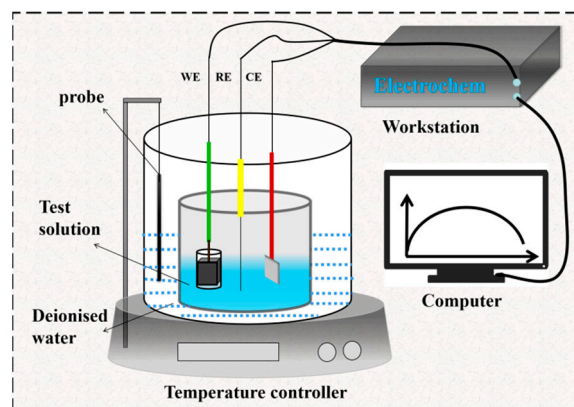
Figure 1. Schematic diagram of electrochemical test equipment.

2.3. Surface Morphology Testing

The Q235 carbon steel was immersed in the test solutions for 6 h. Then, Q235 carbon steel surfaces were observed microscopically and analyzed for composition using a scanning electron microscope (GeminiSEM 500) and EDS spectrometer (Oxford UltimMax 65, ZEISS, Oberkochen, Germany).

2.4. Quantum Chemical Calculations

Optimization of the molecules was achieved with the Gaussian 16 package [18] using the B3LYP function. In this system, the electronic configuration was based on a 6-31 level g* to describe the C, H, N, and O group atoms and the LANL08 basis set for Na. All geometries were confirmed as the minimum through frequency calculations [19]. We calculated the following parameters: the absolute chemical softness (σ), the absolute chemical hardness (η), the electronegativity (χ), the dipole moment (μ), the electrophilicity (ω), the number of transferred electrons (ΔN). The electron affinity (*E.A*) and ionization potential (*I.P*) [20,21]. All calculation relations are as follows:

$$E.A = -E_{LUMO} \tag{1}$$

$$I.P = -E_{HOMO} \tag{2}$$

$$\chi = -\frac{(E_{HOMO} + E_{LUMO})}{2} \tag{3}$$

$$\eta = -\frac{(E_{HOMO} - E_{LUMO})}{2} \tag{4}$$

$$\sigma = \frac{1}{\eta} \tag{5}$$

$$\omega = \frac{\chi^2}{2\eta} \tag{6}$$

$$\Delta N = \frac{X_{Fe} - X_{inh}}{2(\eta_{Fe} - \eta_{inh})} \tag{7}$$

where $\eta_{Fe} = 0$ ev/mol, $X_{Fe} = 7$ ev/mol.

The adsorption mechanism of carbon steel was specifically characterized by determining the active sites of IDS, which were calculated for each atom using the Fukui function. The values f_k were obtained by the finite difference approximation introduced by Yang and Mortier [22]. The nucleophilic attack (f_k^+) and electrophilic attack (f_k^-) are expressed as follows:

$$f_k^+ = q_k(N+1) - q_k(N) \tag{8}$$

$$f_k^- = q_k(N) - q_k(N-1) \tag{9}$$

where $q_k(N+1)$, $q_k(N)$, $q_k(N-1)$ denotes the charge of the anionic, neutral, and cationic types on the k atom, respectively.

The local softness ($\sigma_k^\pm$) and electrophilicity ($\omega_k^\pm$) are calculated as follows [23]:

$$\sigma_k^\pm = \sigma f_k^\pm \tag{10}$$

$$\omega_k^\pm = \omega f_k^\pm \tag{11}$$

The dual local descriptors are a better way to visualize the distribution of molecular activity than the local reaction indexes, and the dual local descriptors are calculated as shown below [24]:

$$f_k^2 = f_k^+ - f_k^- \tag{12}$$

$$\Delta\sigma_k = \sigma_k^+ - \sigma_k^- \tag{13}$$

$$\Delta\omega_k = \omega_k^+ - \omega_k^- \tag{14}$$

2.5. MD Simulations

The molecular dynamics simulations were run with the Material Studio software. We chose more suitable parameters such as the box size of 40.5385 Å × 40.1296 Å × 5.5 Å, containing 500 H_2O, a vacuum layer of 30 Å above the box set up, the NVT system with an Andersen heat bath (298 K), 1 fs time step, time duration of 1000 ps and a reliable COMPASS force field.

3. Results and Discussion

3.1. Open Circuit Potential

The measurement of the Open circuit potential has an essential influence on the reliability of the results of electrochemical impedance tests and polarization curve tests. The curves are presented in Figure 2. The Open circuit potential of Q235 carbon steel immersed in corrosion solution without IDS keeps moving in a negative direction and eventually stabilizes at around 3600 s [25,26]. However, the Open circuit potential with various concentrations of IDS shows a trend of short time increase firstly and then decrease and reaches a stable change at around 3600 s. This is because the IDS inhibitor has a beneficial effect and can produce a film to protect carbon steel. Although, because the high content of aggressive ions in a strongly alkaline environment caused corrosion to occur eventually, a downward trend was observed. Based on the results of this experiment can be obtained, carbon steel in the treatment is completed after treatment, and carbon steel needs to be immersed for at least 1 h to reach stability before continuing to test the EIS and TF.
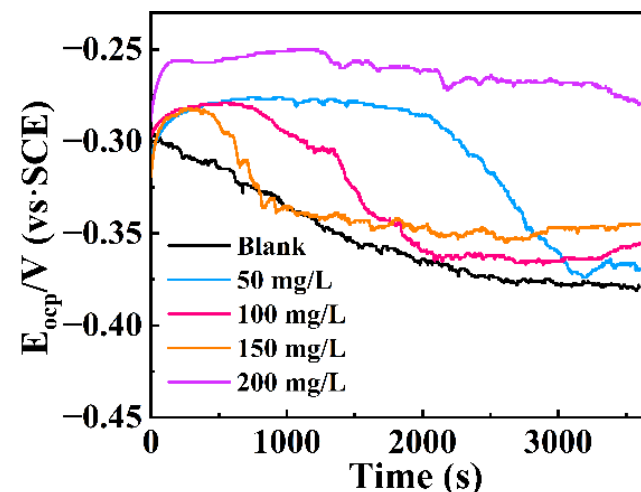

Figure 2. Open circuit potential of Q235 carbon steel.

3.2. Electrochemical Impedance Spectroscopy

Figure 3 represents the Nyquist and Bode plots without and with corrosion inhibitors, respectively. All Nyquist curves demonstrate a single capacitive loop, and the smallest impedance arc radius is shown in Figure 3a without corrosion inhibitor. Impedance arc radius increases with the addition of IDS, and the greater the concentration of IDS, the more obvious the protective behavior. As shown in Figure 3b, we can see the low−frequency impedance value and the maximum phase angle both increase with the addition of IDS, which suggests that the IDS has a good protective effect on carbon steel, a more stable protective layer can be formed on a carbon steel surface to prevent corrosive ions from eroding carbon steel [27–29].
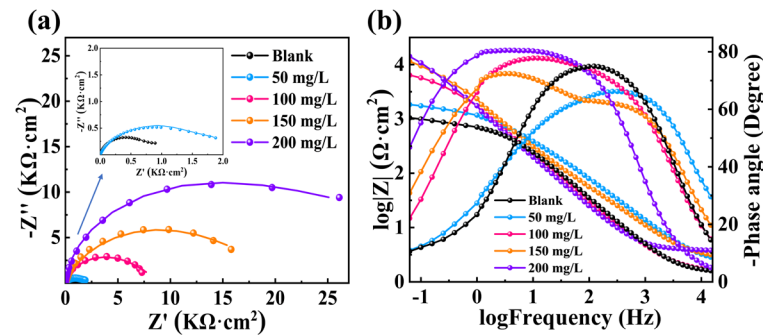

Figure 3. Nyquist (**a**) and Bode (**b**) plots of Q235 carbon steel.

As shown in Figure 4, this equivalent circuit diagram has been used in many articles about corrosion and has been applied several times in alkaline environments [30–32]. For example, in Figure 4, there is a solution resistance (R_s); a thin film resistance (R_f); a charge transfer resistance (R_{ct}), and constant phase angle elements (CPE$_1$ and CPE$_2$). The expression for a constant phase element (CPE) is as follows [33]:

$$Z_{CPE} = Y_0{}^{-1}(j\omega)^{-n} \tag{15}$$

where Y_0 denotes the scaling factor, ω denotes the angular frequency, j denotes the imaginary root, and n can be used as an indicator of surface inhomogeneity ($-1 \leq n \leq 1$) [34]. The double-layer capacitance (C_{dl}) and the inhibition efficiency (IE$_{EIS}$%) are shown below [35]:

$$C_{dl} = Y_0(2\pi f_{max})^{n-1} \tag{16}$$

$$\text{IE}_{EIS}\% = \frac{R_{ct} - R_{ct0}}{R_{ct}} \times 100 \tag{17}$$

where f_{max} indicates the frequency at which the imaginary part of the impedance reaches its maximum value.
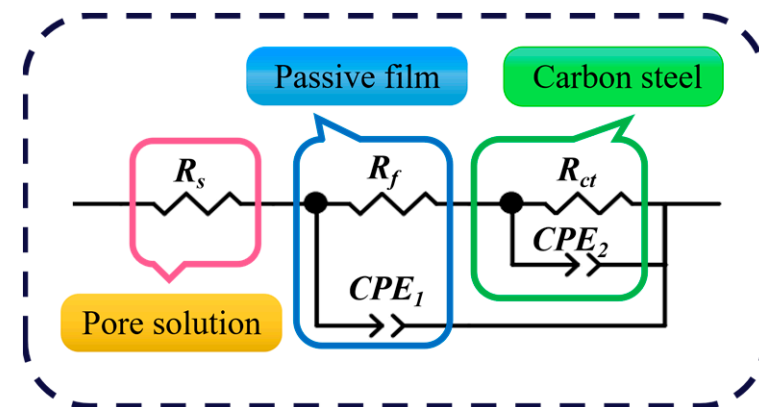

Figure 4. The equivalent circuit diagram.

As shown in Figure 5, the R_{ct} value increases with the increase of IDS concentration, as shown in Table 2, where the corrosion efficiency is 96.79% at 200 mg/L of IDS. In addition, the corrosion-inhibiting effect of IDS can also be expressed by the C_{dl}. We found that the C_{dl} value showed an overall decreasing trend, and usually, the C_{dl} can be expressed by the Helmholtz model as follows [36]:

$$C_{dl} = \frac{\varepsilon_0 \varepsilon}{d} S \tag{18}$$

where d denotes the thickness of the double electric layer, S indicates effective carbon steel area, and ε_0, ε are the vacuum and the dielectric constant of the steel surface. The dielectric constant of the carbon steel surface is reduced after the water molecules are replaced by IDS molecules, and the double electric layer will be thickened. Therefore, the value of C_{dl} will be reduced.
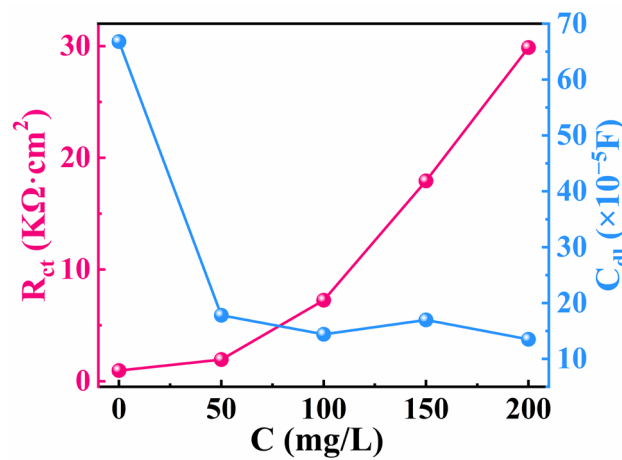

Figure 5. The graph of the variation of R_{ct} and C_{dl}.

Table 2. Impedance parameters of Q235 carbon steel after fitted.

Inhibitor	C (mg/L)	Rs (Ω cm^2)	R_f (Ω cm^2)	Y1 ($\times 10^{-5}$ s^n·ohm^{-1}·cm^{-2})	n^1	R_{ct} (Ω cm^2)	Y2 ($\times 10^{-5}$ s^n·ohm^{-1}·cm^{-2})	n^2	C_{dl} ($\times 10^{-5}$ F)	IE$_{EIS}$%
Blank	0	1.49	697.90	8.99	0.89	957.90	231.19	0.56	66.81	—
IDS	50	1.91	900.30	7.74	0.79	1948.00	65.93	0.36	17.80	50.83
	100	1.53	3024.00	11.62	0.88	7254.00	14.37	0.24	14.41	86.79
	150	2.80	6388.00	6.25	0.86	17,933.00	9.99	0.43	16.99	94.66
	200	3.78	7193.00	7.95	0.97	29,866.00	6.78	0.50	13.51	96.79

3.3. Tafel Polarization Curves

We measured the effect of IDS at different concentrations on carbon steel at 298 K with the Tafel polarization test, as shown in Figure 6. The following parameters are used: corrosion potential (E_{corr}), corrosion current density (I_{corr}), and slope of the curve branches (βc, βa) inhibition efficiency (IE$_{TP}$%) to express the polarization curves [37,38]. The inhibition efficiency (IE$_{TP}$%) was calculated as follows:

$$\text{IE}_{TP}\% = \frac{I_{corr0} - I_{corr}}{I_{corr0}} \times 100 \tag{19}$$

where I_{corr0} and I_{corr} denote the corrosion current density in the absence and presence of IDS. Besides, the rates (CR, mm/year) of carbon steel corrosion were calculated below.

$$\text{CR} = \frac{A \times I_{corr}}{n \times F \times \rho} = 0.0116 \times I_{corr} \tag{20}$$

In the above equation, n denotes the charge transfer number, A denotes iron atomic weight (55.85 g/mol), F represents the Faraday constant (1F = 96,485.33 C/mol), ρ denotes the iron density (7.86 g/cm^3).
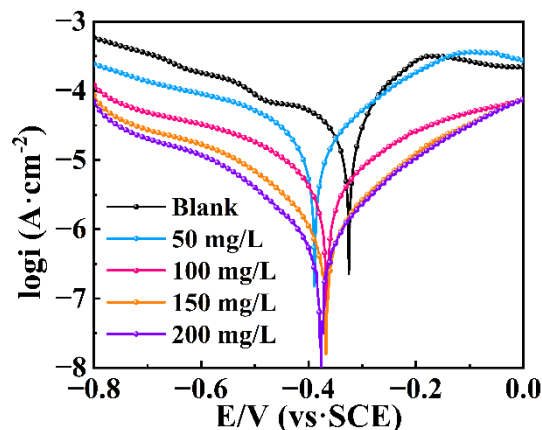
Figure 6. Polarization curves of Q235 carbon steel.

From Figure 6 we can see that the addition of IDS caused the polarization curves to move downward significantly. The polarization curves shifted in the direction of the negative potential. If the E_{corr} of the inhibitor varies by more than 85 mV, it will be classified as an anode or cathode type [39,40]. The value of E_{corr} shifted did not exceed 85 mV, denoting that IDS is a mixed-type inhibitor, inhibiting both anode and cathode. Table 3 illustrates that the values of I_{corr} and CR decrease significantly and the calculated value of $IE_{TP}\%$ increases and the $IE_{TP}\%$ value of IDS reaches 98.30% at 200 mg/L, which can indicate that the greater the concentration of IDS, the stronger the protective effect of the adsorption film.

Table 3. The polarization curve parameters of Q235 steel with different concentrations of IDS.

Inhibitor	C (mg/L)	E_{corr} (V)	βa (mV/Dec)	βc (mV/Dec)	I_{corr} (µA/cm^{-2})	CR (mm/year)	IE_{TP} %
Blank	0	−0.32441	92.79	204.88	22.71	0.263	—
	50	−0.38642	108.25	128.44	9.51	0.110	58.10
IDS	100	−0.35376	141.31	183.74	3.27	0.038	85.62
	150	−0.37065	123.69	117.29	0.71	0.008	96.86
	200	−0.38989	117.36	98.00	0.39	0.004	98.30

According to the electrochemical impedance test and polarization curve test results, the trend of corrosion inhibition efficiency we obtained with the two methods is the same. Table 4 shows the average efficiency. IDS reached the efficiency of 97.54% at 200 mg/L, providing significant protection to the Q235 carbon steel.

Table 4. The average efficiency obtained by combining the two methods.

Inhibitor	C (mg/L)	IE_{EIS} (%)	IE_{TP} (%)	Average of IE (%)
	50	50.83	58.10	54.46
IDS	100	86.79	85.62	86.21
	150	94.66	96.86	95.76
	200	96.79	98.30	97.54

3.4. Adsorption Isotherm Behavior

The adsorption isotherm is of great value in elucidating the form and mechanism of the adsorption of inhibitors. Therefore, we fitted various adsorption curves based on the average of the inhibition efficiencies shown in Table 4 to represent the surface coverage (θ) and used the correlation coefficient to select the most suitable adsorption isotherm for this experiment. As shown in Figure 7, We found that the adsorption of IDS matched the

Langmuir adsorption isotherm (R^2 close to 1). Where the three adsorption isotherms were calculated using these equations [41]:

$$Langmuir : \frac{C}{\theta} = \frac{1}{K_{ads}} + C \tag{21}$$

$$Temkin : exp(-2a\theta) = K_{ads}C \tag{22}$$

$$Frumkin : \frac{\theta}{1-\theta}exp(-2a\theta) = K_{ads}C \tag{23}$$

In these formulas, C denotes the inhibitor content, θ is expressed as the average of the inhibition efficiency (Table 4), and a is the molecular interaction during adsorption. The equilibrium constant (K_{ads}) and the standard Gibbs free energy (ΔG_{ads}) are correlated as follows [42]:
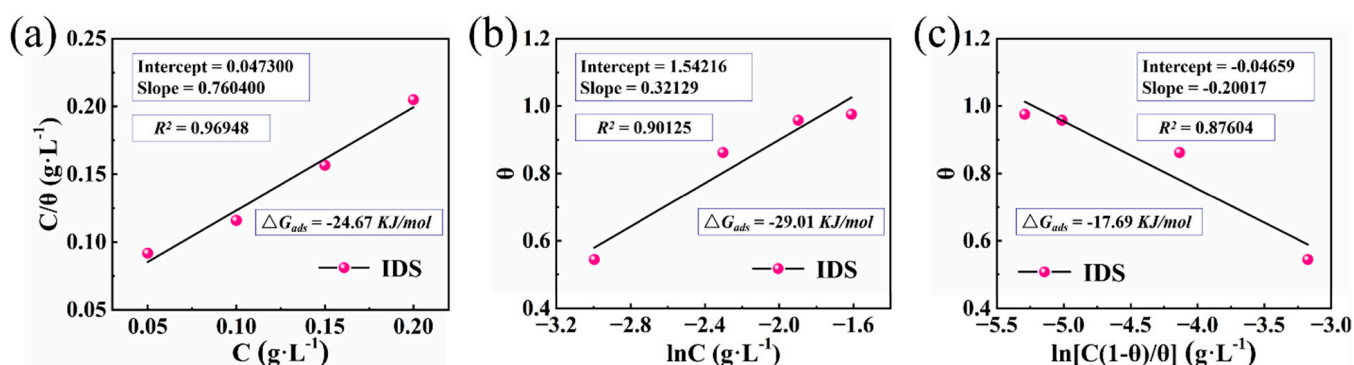
$$\Delta G_{ads} = -RTln\left(1 \times 10^3 K_{ads}\right) \tag{24}$$

Figure 7. Three adsorption models for IDS (**a**) Langmuir, (**b**) Temkin and (**c**) Frumkin.

We can see that the negative value of ΔG_{ads} means that the IDS is spontaneously adsorbed onto carbon steel. The adsorption process is usually divided into physical adsorption and chemisorption. In general, the values of ΔG_{ads} below -20 kJ/mol are physical adsorption, where there is no electron transfer in the process. The values of ΔG_{ads} above -40 kJ/mol are chemisorption due to the bonding of the corrosion inhibitor molecules to the d-space orbitals on the metal surface by means of ligand covalent bonding. Between the two is mixed adsorption [43]. We can see that the value of ΔG_{ads} for IDS is -24.67 KJ/mol, reflecting that IDS protected carbon steel with physical and chemical adsorption. Physical adsorption is the dominant process.

3.5. Surface Studies

Figure 8a,b represent the SEM images of the Q235 carbon steel immersed in the simulated concrete pore solution without inhibitor and containing 200 mg/L IDS for 6h. We can see that the carbon steel surface is rough with deeper cracks and corrosion pits in Figure 8a, indicating that the surface has been attacked. Comparing the SEM image with 200 mg/L IDS added, the cracks and holes are reduced, and the surface is smoother except for the grinding marks. Figure 9a,b shows the corresponding EDS images. Analyzing the two EDS images, we can see the increase of C elements on the surface after adding IDS because it is present in the molecular structure of IDS. The reduction of O and Cl elements and the increase of Fe elements mean that the addition of IDS reduces the number of active sites on the metal surface and decreases the probability of corrosion. Besides, the carbon steel surfaces all have silicon elements left from the sandpaper grinding process.
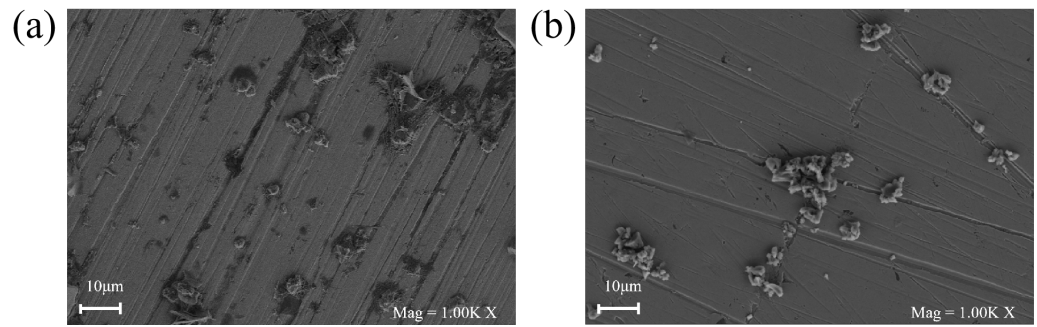
Figure 8. SEM images of Q235 carbon steel (**a**) without IDS (**b**) with 200 mg/L IDS for 6 h.
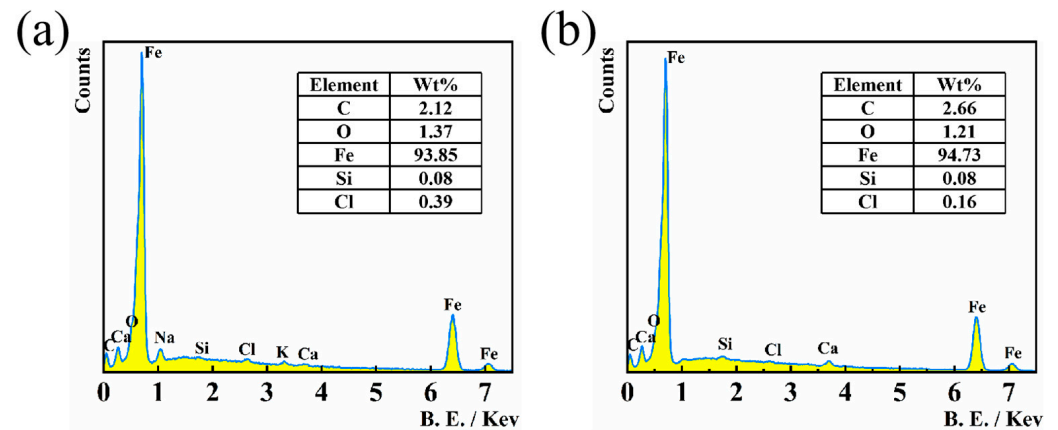

Figure 9. EDS images of Q235 carbon steel (**a**) without IDS (**b**) with 200 mg/L IDS for 6 h.

3.6. Effect of Temperature

Tafel polarization tests were taken to investigate the IDS effect at different temperatures in this work. As shown in Figure 10, we can observe the corrosion current density increases with increasing temperature. From Table 5 and Figure 11a, the efficiency (IE$_{TP}$%) decreases with increasing temperature after adding 200 mg/L IDS, indicating high temperatures accelerate the corrosion and reduce the adsorption of IDS, which means that IDS molecule on the carbon steel substrate desorption occurs, contributing to a decrease in inhibition efficiency [44].
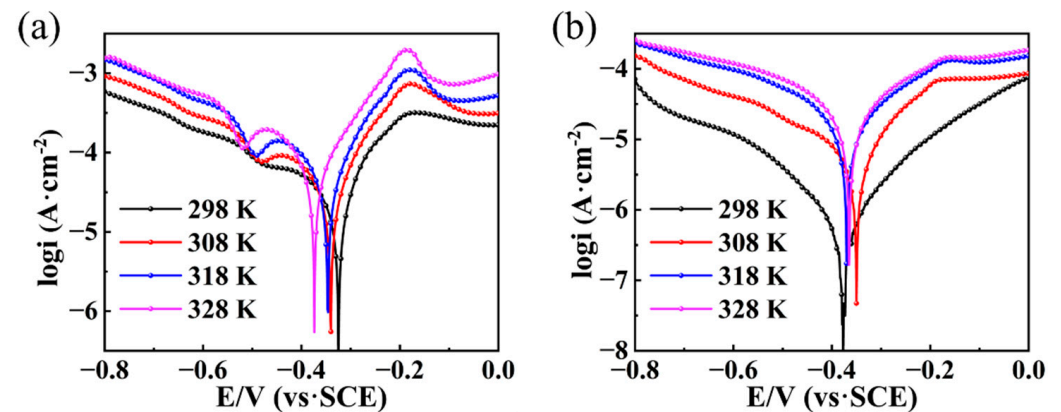

Figure 10. Effect of temperature on the polarization curves of the Q235 carbon steel (**a**) without and (**b**) with 200 mg/L IDS.

Table 5. Polarization parameters for the Q235 carbon steel at different temperatures.

| T	Inhibitor	E_{corr} (V)	βa (mV/Dec)	βc (mV/Dec)	I_{corr} (μA/cm^{-2})	IE_{TP} (%)
298 K	Blank	−0.32441	92.79	204.88	22.71	-
	IDS	−0.38989	117.36	98.00	0.39	98.30
308 K	Blank	−0.32636	59.43	166.72	25.29	-
	IDS	−0.34479	41.39	72.15	1.64	93.53
318 K	Blank	−0.34050	74.73	129.54	33.08	-
	IDS	−0.36863	54.93	57.47	3.98	87.96
328 K	Blank	−0.36870	82.32	112.23	40.70	-
	IDS	−0.36087	65.61	56.74	5.62	86.19

In this work, the activation energy of the carbon steel corrosion process is calculated using the Arrhenius model [45]:

$$I_{corr} = k \cdot exp\frac{-E_a}{RT} \tag{25}$$

The entropy and enthalpy of activation (ΔS_a, ΔH_a) for corrosion dissolution of carbon steel are calculated by the alternative Arrhenius model, as shown in the following equation [45]:

$$I_{corr} = \frac{RT}{hN}exp\left(\frac{\Delta S_a}{R}\right) \cdot \left(\frac{-\Delta H}{RT}\right) \tag{26}$$

In the above equation, N denotes Avogadro's number, E_a denotes the apparent activation energy, R denotes the gas constant, k denotes the pre-exponential factor, h denotes Planck's constant. For example, Figure 11b,c shows the relationship between Log (I_{corr}) and 1/T, Log (I_{corr}/T) and 1/T, and the slopes of the fitted line provide ($-E_a/2.303R$) and ($-\Delta H_a/2.303R$), the intercepts gives (log k) and [log (R/hN) $\Delta S_a/2.303R$] [46].
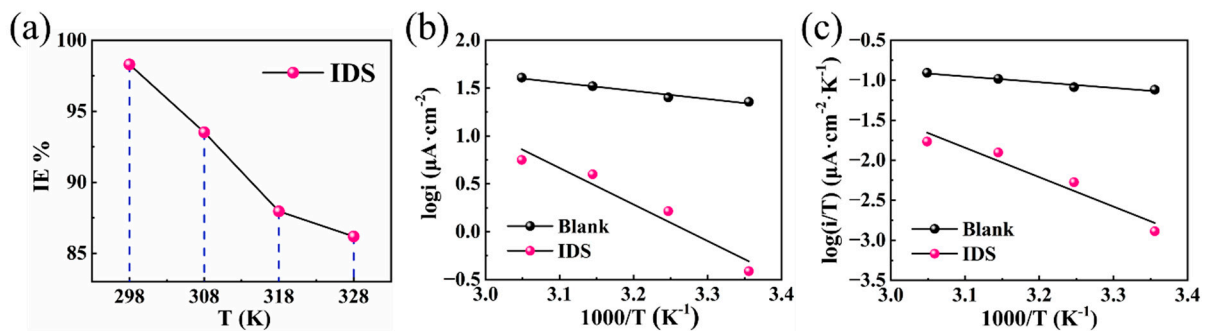
Figure 11. Effect of temperature on the Q235 carbon steel (**a**) Temperature versus corrosion inhibition efficiency, (**b**) Arrhenius plot of log *Icorr* vs. 1/T, (**c**) Transition-state diagram.

The E_a value increases after adding IDS in Table 6, and it can be assumed that the IDS molecules have a strong adsorption capacity, thus inhibiting the corrosion reaction. The positive value of ΔH_a suggests carbon steel is a heat absorption process when dissolved, and ΔH_a (Blank) < ΔH_a (IDS) indicates the dissolution of the carbon steel becomes less after adding IDS. The negative value of ΔS_a suggests that the activation complex is an interaction phase rather than a dissociation phase in the rate-determining phase [47]. The increase in ΔS_a value after adding IDS is due to solvent entropy increase, implying that IDS can form the protective layer [48].

Table 6. Thermodynamic activation parameters of Q235 carbon steel.

Inhibitor	E_a (KJ mol^{-1})	ΔH_a (KJ mol^{-1})	ΔS_a (J mol^{-1} K^{-1})
Blank	16.34	13.75	−173.19
IDS	73.02	70.42	−14.58

3.7. DFT Calculations

The energy (E_{HOMO}, E_{LUMO}) is instrumental in predicting the adsorption center in an inhibitor molecule. The value of E_{HOMO} is related to an inhibitor molecule's ability to give electrons, the value of E_{LUMO} is related to an inhibitor molecule's ability to accept electrons, ΔE is an energy difference between two orbitals, a low ΔE indicates the molecule is less stable and more likely to be involved in binding [49,50]. Figure 12 shows that the electron density distribution (HOMO) is located in the amino group. The carbon atom is attached to the amino group. In contrast, the electron density distribution (LUMO) is mainly located in the sodium group of carboxylic acid. Positive and negative electrostatic potentials are shown in green and blue in the electrostatic potential diagram. For the IDS molecule, the negative ESP region is located around the Na atoms (sodium groups of carboxylic acid), while the positive ESP region is concentrated around the C atoms. Thus, it can be shown that the sodium groups of carboxylic acid in the IDS molecule are important in the electrophile attack and easily form chemical bonds with Fe atoms.
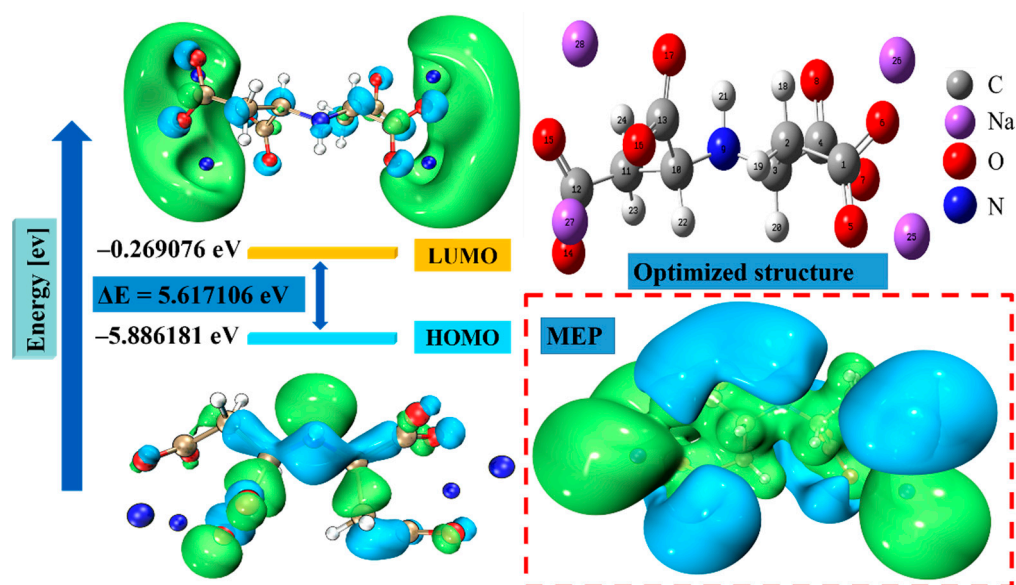

Figure 12. Optimized structure, MESP surface, HOMO surface, and LUMO surface of IDS inhibitor.

The theoretical chemical parameters of the IDS are listed in Table 7. Generally, organic inhibitors with low hardness (η) values and high softness (σ) values adsorb well on metal surfaces. Lukovits' study revealed that the corrosion inhibition efficiency of the inhibitor increases with the increase of the molecular electron supply ability for $\Delta N < 3.6$ [51]. The ΔN we obtained by calculation is less than 3.6, indicating that the IDS inhibitor is more likely to transfer electrons to the carbon steel surface. Furthermore, the dipole moments (μ) we calculated have high values, confirming the high inhibition efficiency of IDS [52].

We used the Fukui index to study the specific reaction sites of IDS molecules in the adsorption process. Higher f_k^- values indicate atoms with a high electron-giving capacity and a high reactivity to participate in the electron-philic attack, while higher f_k^+ values indicate atoms with high reactivity to participate in nucleophilic reactions [53]. The Fukui Index is summarised in Table 8. The results show that for the IDS molecule, the higher f_k^+ values were distributed among the Na28, Na25, Na26, Na27 atoms on the sodium carboxylate group, the higher f_k^- values were distributed among the N9 atom in the amino group and the O16 and O5 atoms in the sodium carboxylate group. These atoms have a strong ability to accept and give electrons, respectively. The active sites are further observed by the dual local descriptors as shown in Figure 13. If the values (f_k^2, $\Delta\sigma_k$ and $\Delta\omega$) of the sites are less than 0, the process prefers electrophilic attack, but if the values (f_k^2, $\Delta\sigma_k$ and $\Delta\omega$) of the sites > 0, the process prefers nucleophilic attack [23]. In Figure 13, the order of

the most active sites giving electrons is: N9 > O16 > O5, and the trend of electron-accepting ability is Na28 > Na25 > Na26 > Na27.

Table 7. The theoretical chemical parameters of IDS.

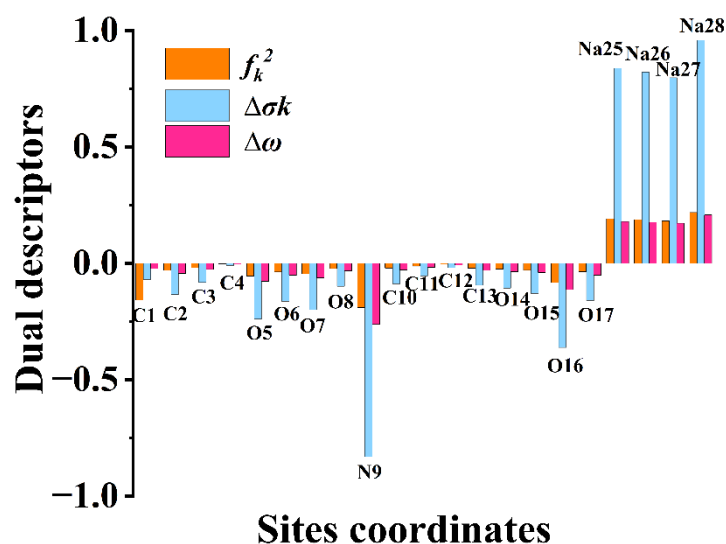| Descriptor	IDS
E_{HOMO} (ev)	−5.88618
E_{LUMO} (ev)	−0.26908
I.P (ev)	5.88618
E.A (ev)	0.26908
ΔE (ev)	5.61711
χ (ev)	3.07763
η (ev)	2.80855
σ (ev^{-1})	0.35606
ω	1.68624
ΔN	0.69829
μ (Debye)	6.74497

Figure 13. The dual descriptors for the most active sites of IDS.

Table 8. Dual local descriptors, Fukui functions, local softness, electrophilicity of IDS.

Atoms	f_k^+	f_k^-	f_k^2	σ_k^+	σ_k^-	$\Delta\sigma_k$	ω^+	ω^-	$\Delta\omega$
1(C)	0.0028	0.0186	−0.158	0.0125	0.0817	−0.0692	0.0029	0.02571	−0.02281
2(C)	0.0014	0.0319	−0.0305	0.006	0.1399	−0.1339	0.00139	0.04410	−0.04271
3(C)	0.0015	0.02	−0.0186	0.0065	0.088	−0.0815	0.00152	0.02765	−0.02613
4(C)	0.0032	0.0052	−0.002	0.0142	0.0228	−0.0086	0.0033	0.00719	−0.00389
5(O)	0.0065	0.0609	−0.0544	0.0286	0.2675	−0.2389	0.00665	0.08419	−0.07754
6(O)	−0.0026	0.0345	−0.0371	−0.0113	0.1516	−0.1629	−0.00263	0.04769	−0.05032
7(O)	−0.0021	0.0432	−0.0452	−0.009	0.1896	−0.1986	−0.0021	0.05972	−0.06182
8(O)	0.0056	0.028	−0.0224	0.0246	0.123	−0.0984	0.00573	0.03871	−0.03298
9(N)	0.0042	0.1933	−0.1891	0.0183	0.8485	−0.8302	0.00426	0.26722	−0.26296
10(C)	0.0015	0.0216	−0.0201	0.0064	0.0947	−0.0883	0.00149	0.02986	−0.02837
11(C)	0.0034	0.0157	−0.0124	0.0149	0.0691	−0.0542	0.00347	0.02170	−0.01823
12(C)	0.0041	0.0084	−0.0042	0.0182	0.0367	−0.0185	0.00423	0.01161	−0.00738
13(C)	0.0016	0.0228	−0.0213	0.007	0.1003	−0.0933	0.00162	0.03152	−0.02990
14(O)	0.0085	0.0326	−0.0242	0.0372	0.1433	−0.1061	0.00865	0.04507	−0.03642
15(O)	−0.0038	0.0257	−0.0295	−0.0165	0.1128	−0.1293	−0.00385	0.03553	−0.03938
16(O)	−0.0032	0.0791	−0.0823	−0.0139	0.3472	−0.3611	−0.00325	0.10935	−0.11260
17(O)	0.003	0.0395	−0.0364	0.0133	0.1732	−0.1599	0.00311	0.05460	−0.05149
25(Na)	0.2344	0.0435	0.1908	1.029	0.1911	0.8379	0.23956	0.06013	0.17943
26(Na)	0.2276	0.0405	0.1871	0.9992	0.1778	0.8214	0.23264	0.05599	0.17665
27(Na)	0.2197	0.0381	0.1817	0.9647	0.1672	0.7975	0.2246	0.05267	0.17193
28(Na)	0.2611	0.0427	0.2184	1.1463	0.1874	0.9589	0.26689	0.05903	0.20786

3.8. MD Simulations

Figure 14a,b represents the side and top views of the stable equilibrium configuration of IDS adsorbed on the surface of Fe (110), respectively, it can be seen that the sodium carboxylate groups and N atoms of IDS molecules are preferentially adsorbed on the surface. The adsorption energy (E_{ads}) is expressed as follows [28,54]:

$$E_{ads} = E_{total} - E_{surface} - E_{inhibitor} \tag{27}$$

where E_{total} represents the total energy, $E_{surface}$ represents the energy of Fe, and $E_{inhibitor}$ represents that of the inhibitor molecule. The calculated adsorption energy is negative in Table 9, which further indicates that IDS is spontaneously adsorbed on the surface.
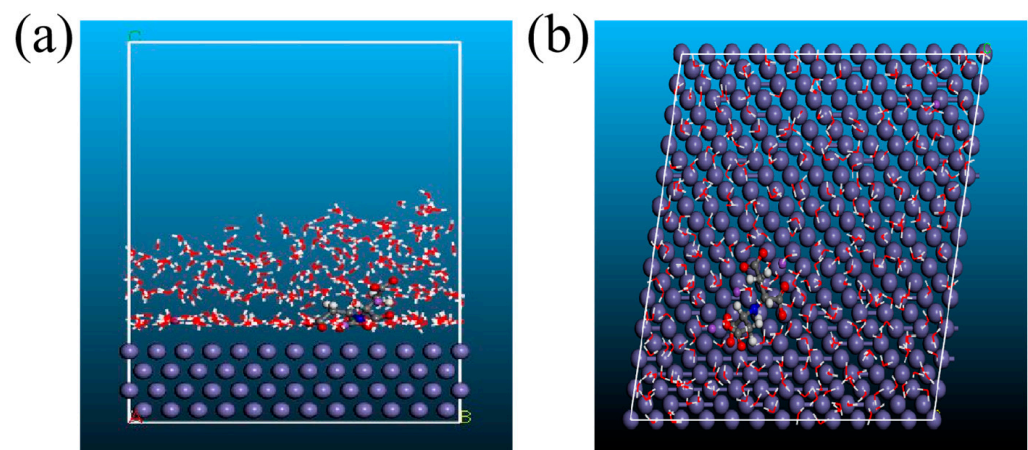

Figure 14. Side (**a**) and top (**b**) views of stable equilibrium configuration of IDS.

Table 9. The activation parameters of Q235 carbon steel.

E_{total} (kcal/mol)	$E_{surface}$ (kcal/mol)	$E_{inhibitor}$ (kcal/mol)	E_{ads} (kcal/mol)
−55,044.77	−54,499.59	−472.04	−73.14

It is well known that corrosion occurs when water molecules in the air attach to the carbon steel surface, and the addition of IDS will replace the water molecules, thus inhibiting the corrosion of carbon steel. We can see from Figure 15a that the density of water molecules with the addition of IDS decreases within 20 Å, which is consistent with our experimental results.
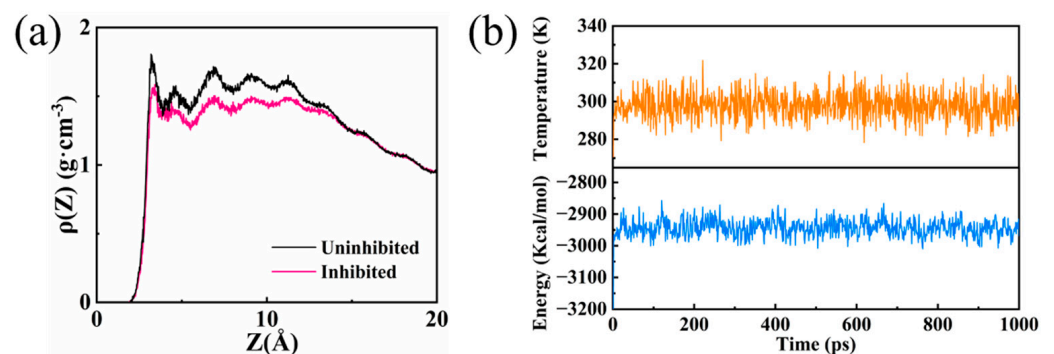

Figure 15. (**a**) Density changes curves for water on carbon steel without and with IDS, (**b**) Variation of temperature (yellow) and energy (blue) at different AIMD times.

3.9. Mechanism of Inhibition

The IDS inhibitor protects carbon steel through physical and chemical adsorption in this work. Figure 16a shows the carbon steel surface was attacked by chloride ions and suffered severe corrosion when no inhibitor was added. Figure 16b represents the inhibition of carbon steel by adding IDS. The physical adsorption process means that the positive charges in the IDS molecules adsorb to the surface. As a result, the protective film formed at the carbon steel-solution interface protects the carbon steel, reducing the diffusion of oxygen and the entry of aggressive ions and water molecules. The chemisorption process refers to the interaction between the –COONa groups and the N atoms of the IDS and the empty d-orbitals of the Fe atoms on the carbon steel surface, forming covalent bonds and covering the surface, enhancing the protective effect.
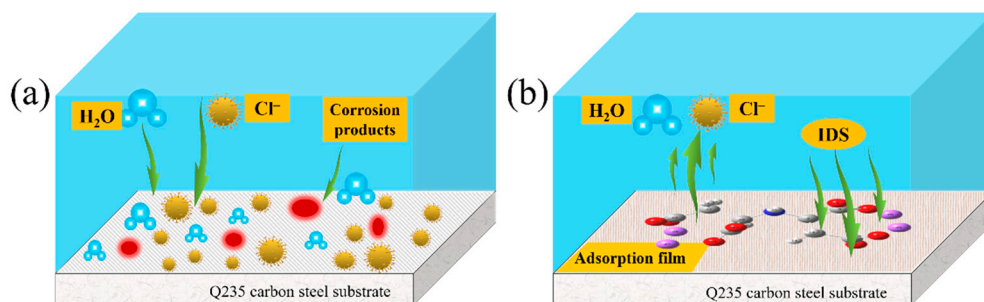

Figure 16. Schematic diagram of the corrosion inhibitor mechanism on steel in simulated concrete pore fluid: (**a**) blank, (**b**) IDS.

3.10. Comparison of Similar Corrosion Inhibitors

We compared IDS with reported corrosion inhibitors like its molecular structure, and the inhibition effects derived from the comparison are summarized in Table 10. As a result, we can obtain that IDS exhibits the highest corrosion inhibition effect. Without adding any auxiliary conditions, our reported IDS reaches an efficiency of 97.54% at 200 mg/L, which is higher than the corrosion efficiency of corrosion inhibitors reported in similar environments. This indicates that IDS is of good research value in the field of corrosion and can be used as an efficient corrosion inhibitor.

Table 10. Comparison of the protection efficiency of IDS with corrosion inhibitors of similar molecular structure for carbon steel.

Inhibitor			
Metal	mild steel	Q235 carbon steel	Q235 carbon steel
Corrosive media	Aerated 3% NaCl solution	0.5 M NaCl simulated concrete pore solution	3.5% NaCl simulated concrete pore solution
Optimum concentration	2 mg/L Zn^+ + 2 mg/L PESA	0.1 M	200 mg/L
Protection efficiency	92%	91%	97.54%
References	[13]	[15]	In this work

4. Conclusions

We investigated the inhibition effect and mechanism of IDS through a series of test methods and calculations. At last, we have found several conclusions:

1. The ddouble-layer capacitance (C_{dl}) was significantly reduced, and the charge transfer resistance (R_{ct}) was significantly increased after adding IDS. This demonstrates that corrosion of Q235 carbon steel can be effectively retarded when adding IDS to the simulated concrete solution.
2. IDS acts on both the cathode and anode of Q235 carbon steel, the IDS efficiency reached 97.54% at 200 mg/L.
3. IDS on carbon steel surface is spontaneous, mainly physical adsorption, which matches the Langmuir adsorption model well.
4. The DFT and MD simulations support the results of the tests and further indicate the sodium carboxylate groups in the IDS molecule play a major role in the corrosion inhibition process. It can be used as a new type of highly efficient inhibitor.

References

1. Tang, Y.; Miao, Y.; Zuo, Y.; Zhang, G.; Wang, C. Corrosion behavior of steel in simulated concrete pore solutions treated with calcium silicate hydrates. *Constr. Build. Mater.* **2011**, *30*, 252–256. [CrossRef]
2. Ben Mansour, H.; Dhouibi, L.; Idrissi, H. Effect of Phosphate-based inhibitor on prestressing tendons corrosion in simulated concrete pore solution contaminated by chloride ions. *Constr. Build. Mater.* **2018**, *171*, 250–260. [CrossRef]
3. Rathod, M.R.; Rajappa, S.; Minagalavar, R.L.; Praveen, B.; Devendra, B.K.; Kittur, A. Investigation of African mangosteen leaves extract as an environment-friendly inhibitor for low carbon steel in 0.5 M H2SO4. *Inorg. Chem. Commun.* **2022**, *140*, 109488. [CrossRef]
4. Matad, P.B.; Mokshanatha, P.B.; Hebbar, N.; Venkatesha, V.T.; Tandon, H.C. Ketosulfone Drug as a Green Corrosion Inhibitor for Mild Steel in Acidic Medium. *Ind. Eng. Chem. Res.* **2014**, *53*, 8436–8444. [CrossRef]
5. Hebbar, N.; Praveen, B.; Prasanna, B.; Vishwanath, P. Electrochemical and Adsorption Studies of 4-Chloro, 8-(Trifluoromethyl) Quinoline (CTQ) for Mild Steel in Acidic Medium. *J. Fail. Anal. Prev.* **2020**, *20*, 1516–1523. [CrossRef]
6. Bryan, N.S.; Alexander, D.D.; Coughlin, J.R.; Milkowski, A.L.; Boffetta, P. Ingested nitrate and nitrite and stomach cancer risk: An updated review. *Food Chem. Toxicol.* **2012**, *50*, 3646–3665. [CrossRef]
7. Praveen, B.M.; Alhadhrami, A.; Prasanna, B.M.; Hebbar, N.; Prabhu, R. Anti-Corrosion Behavior of Olmesartan for Soft-Cast Steel in 1 mol dm^{-3} HCl. *Coatings* **2021**, *11*, 965. [CrossRef]
8. Lin, B.; Zuo, Y. Corrosion inhibition of carboxylate inhibitors with different alkylene chain lengths on carbon steel in an alkaline solution. *RSC Adv.* **2019**, *9*, 7065–7077. [CrossRef]
9. Wysocka, J.; Cieslik, M.; Krakowiak, S.; Ryl, J. Carboxylic acids as efficient corrosion inhibitors of aluminium alloys in alkaline media. *Electrochim. Acta* **2018**, *289*, 175–192. [CrossRef]
10. Praveen, B.; Prasanna, B.; Mallikarjuna, N.; Jagadeesh, M.; Hebbar, N.; Rashmi, D. Investigation of anticorrosive behaviour of novel tert-butyl 4-[(4-methyl phenyl) carbonyl] piperazine-1-carboxylate for carbon steel in 1M HCl. *Heliyon* **2021**, *7*, e06090. [CrossRef]
11. Faisal, M.; Saeed, A.; Shahzad, D.; Abbas, N.; Larik, F.A.; Channar, P.A.; Fattah, T.A.; Khan, D.M.; Shehzadi, S.A. General properties and comparison of the corrosion inhibition efficiencies of the triazole derivatives for mild steel. *Corros. Rev.* **2018**, *36*, 507–545. [CrossRef]

12. Marzorati, S.; Verotta, L.; Trasatti, S.P. Green Corrosion Inhibitors from Natural Sources and Biomass Wastes. *Molecules* **2018**, *24*, 48. [CrossRef]

13. Zeino, A.; Abdulazeez, I.; Khaled, M.; Jawish, M.W.; Obot, I.; Alhooshani, K. Mechanistic study of polyepoxy succinic acid (PESA) as green corrosion inhibitor on carbon steel in aerated NaCl Solution. *Mater. Today Commun.* **2021**, *29*, 102848. [CrossRef]

14. Azamian, I.; Allahkaram, S.; Johari, M.; Teymouri, F. Interfacial Interaction Study of EDTA with the Defect Structure of Fe 3-δ O 4 Passive Film in an Aggressive Alkaline Medium Based on the Lattice Theory of Point Defects. *RSC Adv.* **2022**, *12*, 3524–3541. [CrossRef]

15. Teymouri, F.; Allahkaram, S.R.; Shekarchi, M.; Azamian, I.; Johari, M. A comprehensive study on the inhibition behaviour of four carboxylate-based corrosion inhibitors focusing on efficiency drop after the optimum concentration for carbon steel in the simulated concrete pore solution. *Constr. Build. Mater.* **2021**, *296*, 123702. [CrossRef]

16. Lashgari, S.M.; Bahlakeh, G.; Ramezanzadeh, B. Detailed theoretical DFT computation/molecular simulation and electrochemical explorations of Thymus vulgaris leave extract for effective mild-steel corrosion retardation in HCl solution. *J. Mol. Liq.* **2021**, *335*, 115897. [CrossRef]

17. Zhang, Z.; Ba, H.; Wu, Z.; Zhu, Y. The inhibition mechanism of maize gluten meal extract as green inhibitor for steel in concrete via experimental and theoretical elucidation. *Constr. Build. Mater.* **2018**, *198*, 288–298. [CrossRef]

18. Frisch, M.J.; Trucks, G.W.; Schlegel, H.B.; Scuseria, G.E.; Robb, M.A.; Cheeseman, J.R.; Scalmani, G.; Barone, V.; Petersson, G.A.; Nakatsuji, H.; et al. *Gaussian 16*, Revision C.01; Gaussian Inc.: Wallingford, CT, USA, 2016.

19. Zhang, Q.; Jiang, Z.; Li, Y.; Wang, X.; Xiong, W.; Liu, H.; Zhang, G. In-Depth Insight into the Inhibition Mechanism of the Modified and Combined Amino Acids Corrosion Inhibitors: "Intramolecular Synergism" vs. "Intermolecular Synergism". *Chem. Eng. J.* **2022**, *437*, 135439. [CrossRef]

20. Al Zoubi, W.; Ko, Y.G. Self-assembly of hierarchical N-heterocycles-inorganic materials into three-dimensional structure for superior corrosion protection. *Chem. Eng. J.* **2018**, *356*, 850–856. [CrossRef]

21. Ouakki, M.; Galai, M.; Rbaa, M.; Abousalem, A.; Lakhrissi, B.; Rifi, E.; Cherkaoui, M. Quantum chemical and experimental evaluation of the inhibitory action of two imidazole derivatives on mild steel corrosion in sulphuric acid medium. *Heliyon* **2019**, *5*, e02759. [CrossRef]

22. Yang, W.; Mortier, W.J. The use of global and local molecular parameters for the analysis of the gas-phase basicity of amines. *J. Am. Chem. Soc.* **1986**, *108*, 5708–5711. [CrossRef]

23. Hsissou, R. Review on epoxy polymers and its composites as a potential anticorrosive coatings for carbon steel in 3.5% NaCl solution: Computational approaches. *J. Mol. Liq.* **2021**, *336*, 116307. [CrossRef]

24. Hsissou, R.; Abbout, S.; Benhiba, F.; Seghiri, R.; Safi, Z.; Kaya, S.; Briche, S.; Serdaroğlu, G.; Erramli, H.; Elbachiri, A.; et al. Insight into the Corrosion Inhibition of Novel Macromolecular Epoxy Resin as Highly Efficient Inhibitor for Carbon Steel in Acidic Mediums: Synthesis, Characterization, Electrochemical Techniques, AFM/UV–Visible and Computational Investigations. *J. Mol. Liq.* **2021**, *337*, 116492. [CrossRef]

25. Wu, Y.; Yu, J.; Zhao, W.; Wang, C.; Wu, B.; Lu, G. Investigating the anti-corrosion behaviors of the waterborne epoxy composite coatings with barrier and inhibition roles on mild steel. *Prog. Org. Coat.* **2019**, *133*, 8–18. [CrossRef]

26. Javidparvar, A.A.; Naderi, R.; Ramezanzadeh, B. Epoxy-polyamide nanocomposite coating with graphene oxide as cerium nanocontainer generating effective dual active/barrier corrosion protection. *Compos. Part B Eng.* **2019**, *172*, 363–375. [CrossRef]

27. Kornblum, N.; Blackwood, R.K.; Mooberry, D.D. The Reaction of Aliphatic Nitro Compounds with Nitrite Esters[1,2]. *J. Am. Chem. Soc.* **1956**, *78*, 1501–1504. [CrossRef]

28. Wang, Q.; Fu, S.; Yang, X.; Sun, Q.; Zhang, J.; Peng, Y.; Zhang, R.; Liang, Z.; Li, J. An imide-based organic polymer as an inhibitor for HRB400 steel in simulated concrete pore solution: Experimental and theoretical calculations. *J. Mol. Struct.* **2022**, *1265*, 133426. [CrossRef]

29. Qiu, S.; Li, W.; Zheng, W.; Zhao, H.; Wang, L. Synergistic Effect of Polypyrrole-Intercalated Graphene for Enhanced Corrosion Protection of Aqueous Coating in 3.5% NaCl Solution. *ACS Appl. Mater. Interfaces* **2017**, *9*, 34294–34304. [CrossRef]

30. Obot, I.; Macdonald, D.; Gasem, Z. Density functional theory (DFT) as a powerful tool for designing new organic corrosion inhibitors. Part 1: An overview. *Corros. Sci.* **2015**, *99*, 1–30. [CrossRef]

31. Peme, T.; Olasunkanmi, L.O.; Bahadur, I.; Adekunle, A.S.; Kabanda, M.M.; Ebenso, E.E. Adsorption and Corrosion Inhibition Studies of Some Selected Dyes as Corrosion Inhibitors for Mild Steel in Acidic Medium: Gravimetric, Electrochemical, Quantum Chemical Studies and Synergistic Effect with Iodide Ions. *Molecules* **2015**, *20*, 16004–16029. [CrossRef]

32. Ma, X.; Xu, L.; Wang, W.; Lin, Z.; Li, X. Synthesis and characterisation of composite nanoparticles of mesoporous silica loaded with inhibitor for corrosion protection of Cu-Zn alloy. *Corros. Sci.* **2017**, *120*, 139–147. [CrossRef]

33. Ansari, K.R.; Quraishi, M.A.; Singh, A.; Ramkumar, S.; Obote, I.B. Corrosion inhibition of N80 steel in 15% HCl by pyrazolone derivatives: Electrochemical, surface and quantum chemical studies. *RSC Adv.* **2016**, *6*, 24130–24141. [CrossRef]

34. Umoren, S.A.; Gasem, Z.M.; Obot, I.B. Natural Products for Material Protection: Inhibition of Mild Steel Corrosion by Date Palm Seed Extracts in Acidic Media. *Ind. Eng. Chem. Res.* **2013**, *52*, 14855–14865. [CrossRef]

35. Peimani, A.; Nasr-Esfahani, M. Application of Anise Extract for Corrosion Inhibition of Carbon Steel in CO_2 Saturated 3.0% NaCl Solution. *Prot. Met. Phys. Chem. Surfaces* **2018**, *54*, 122–134. [CrossRef]

36. Singh, A.; Ansari, K.; Quraishi, M.; Lgaz, H.; Lin, Y. Synthesis and investigation of pyran derivatives as acidizing corrosion inhibitors for N80 steel in hydrochloric acid: Theoretical and experimental approaches. *J. Alloys Compd.* **2018**, *762*, 347–362. [CrossRef]

37. Ituen, E.B.; Akaranta, O.; Umoren, S.A. N-acetyl cysteine based corrosion inhibitor formulations for steel protection in 15% HCl solution. *J. Mol. Liq.* **2017**, *246*, 112–118. [CrossRef]

38. Singh, P.; Chauhan, D.; Chauhan, S.; Singh, G.; Quraishi, M. Chemically modified expired Dapsone drug as environmentally benign corrosion inhibitor for mild steel in sulphuric acid useful for industrial pickling process. *J. Mol. Liq.* **2019**, *286*, 110903. [CrossRef]

39. El Aatiaoui, A.; Koudad, M.; Chelfi, T.; Erkan, S.; Azzouzi, M.; Aouniti, A.; Savaş, K.; Kaddouri, M.; Benchat, N.; Oussaid, A. Experimental and Theoretical Study of New Schiff Bases Based on Imidazo (1, 2-a) Pyridine as Corrosion Inhibitor of Mild Steel in 1M HCl. *J. Mol. Struct.* **2021**, *1226*, 129372. [CrossRef]

40. Domínguez-Crespo, M.; García-Murillo, A.; Torres-Huerta, A.; Carrillo-Romo, F.; Onofre-Bustamante, E.; Yáñez-Zamora, C. Characterization of ceramic sol–gel coatings as an alternative chemical conversion treatment on commercial carbon steel. *Electrochim. Acta* **2009**, *54*, 2932–2940. [CrossRef]

41. Myung, N.V.; Park, D.-Y.; Yoo, B.-Y.; Sumodjo, P.T. Development of electroplated magnetic materials for MEMS. *J. Magn. Magn. Mater.* **2003**, *265*, 189–198. [CrossRef]

42. Zhang, Z.; Ba, H.; Wu, Z. Sustainable corrosion inhibitor for steel in simulated concrete pore solution by maize gluten meal extract: Electrochemical and adsorption behavior studies. *Constr. Build. Mater.* **2019**, *227*, 117080. [CrossRef]

43. Fernandes, C.M.; Alvarez, L.X.; dos Santos, N.E.; Barrios, A.C.M.; Ponzio, E.A. Green synthesis of 1-benzyl-4-phenyl-1H-1,2,3-triazole, its application as corrosion inhibitor for mild steel in acidic medium and new approach of classical electrochemical analyses. *Corros. Sci.* **2019**, *149*, 185–194. [CrossRef]

44. Madkour, L.H.; Kaya, S.; Obot, I.B. Computational, Monte Carlo simulation and experimental studies of some arylazotriazoles (AATR) and their copper complexes in corrosion inhibition process. *J. Mol. Liq.* **2018**, *260*, 351–374. [CrossRef]

45. Bellal, Y.; Benghanem, F.; Keraghel, S. A new corrosion inhibitor for steel rebar in concrete: Synthesis, electrochemical and theoretical studies. *J. Mol. Struct.* **2020**, *1225*, 129257. [CrossRef]

46. Badiea, A.M.; Mohana, K.N. Effect of fluid velocity and temperature on the corrosion mechanism of low carbon steel in industrial water in the absence and presence of 2-hydrazino benzothiazole. *Korean J. Chem. Eng.* **2008**, *25*, 1292–1299. [CrossRef]

47. Tawfik, S.M. Ionic liquids based gemini cationic surfactants as corrosion inhibitors for carbon steel in hydrochloric acid solution. *J. Mol. Liq.* **2016**, *216*, 624–635. [CrossRef]

48. Dehghani, A.; Bahlakeh, G.; Ramezanzadeh, B. Green Eucalyptus leaf extract: A potent source of bio-active corrosion inhibitors for mild steel. *Bioelectrochemistry* **2019**, *130*, 107339. [CrossRef]

49. Belghiti, M.; Echihi, S.; Dafali, A.; Karzazi, Y.; Bakasse, M.; Elalaoui-Elabdallaoui, H.; Olasunkanmi, L.; Ebenso, E.; Tabyaoui, M. Computational simulation and statistical analysis on the relationship between corrosion inhibition efficiency and molecular structure of some hydrazine derivatives in phosphoric acid on mild steel surface. *Appl. Surf. Sci.* **2019**, *491*, 707–722. [CrossRef]

50. Madkour, L.H.; Kaya, S.; Guo, L.; Kaya, C. Quantum chemical calculations, molecular dynamic (MD) simulations and experimental studies of using some azo dyes as corrosion inhibitors for iron. Part 2: Bis–azo dye derivatives. *J. Mol. Struct.* **2018**, *1163*, 397–417. [CrossRef]

51. Lukovits, I.; Kálmán, E.; Zucchi, F. Corrosion Inhibitors—Correlation between Electronic Structure and Efficiency. *Corrosion* **2001**, *57*, 3–8. [CrossRef]

52. Kokalj, A. Is the analysis of molecular electronic structure of corrosion inhibitors sufficient to predict the trend of their inhibition performance. *Electrochim. Acta* **2010**, *56*, 745–755. [CrossRef]

53. Ghailane, T.; Balkhmima, R.; Ghailane, R.; Souizi, A.; Touir, R.; Touhami, M.E.; Marakchi, K.; Komiha, N. Experimental and theoretical studies for mild steel corrosion inhibition in 1M HCl by two new benzothiazine derivatives. *Corros. Sci.* **2013**, *76*, 317–324. [CrossRef]

54. Zhu, J.; Zhou, G.; Niu, F.; Shi, Y.; Du, Z.; Lu, G.; Liu, Z. Understanding the inhibition performance of novel dibenzimidazole derivatives on Fe (110) surface: DFT and MD simulation insights. *J. Mater. Res. Technol.* **2022**, *17*, 211–222. [CrossRef]